Rare Met. (2023) 42(7):2381–2389
https://doi.org/10.1007/s12598-018-1181-0

RARE METALS
www.editorialmanager.com/rmet

Strain-controlled fatigue characteristics of a cast Mg–Nd–Zn under peak-aged and over-aged conditions

Zhen-Ming Li, Ji-Chun Dai, Bao-Liang Liu*, Hui Zou, Ji-Peng Pan

Received: 15 July 2017 / Revised: 9 October 2017 / Accepted: 28 October 2018 / Published online: 7 December 2018

Abstract Strain-controlled fatigue characteristics of peak-aged and over-aged $Mg_{96.47}Nd_{2.9}Zn_{0.21}$ magnesium alloys containing 0.42Zr, including stress response, strain resistance, hysteresis loops, strain–life and corresponding low-cycle fatigue life prediction model, were studied. In the peak-aged state ($T6_1$: 540 °C × 8 h + 200 °C × 14 h), the alloy shows higher cyclic stress response, but lower ductility than the alloy in the over-aged state ($T6_2$: 540 °C × 8 h + 200 °C × 400 h). The yield strength and ultimate tensile strength of the alloy under $T6_1$- and $T6_2$-treated conditions are close. Compared with $T6_1$-treated alloy, the steady stress amplitude occurred in $T6_2$-treated alloy is due to higher ductility and more homogenous deformation. In $T6_1$ state, the fatigue cracks in the alloy first initiate along the cracked persistent slip bands and then propagate in the trans-granular mode, while in the $T6_2$ state, the fatigue cracks initiate along grain boundaries and then propagate in the inter-granular mode.

Keywords Mg–Nd–Zn alloy; Strain-controlled fatigue; Peak-aged and over-aged conditions; Hysteresis energy

1 Introduction

Magnesium alloys have been attractive for aerospace and transportation industries because they are the lightest structural metals, and thus, producing components by them could remarkably reduce weight and fuel consumption [1–3]. Among magnesium alloys, the rare earth (RE) element-containing system possesses improved comprehensive performances such as mechanical properties [4–7], casting properties [8] and damping performances [9, 10]. Fatigue property is important for metals because fatigue failure is a main type of failure mode for metal parts [11–13]. Therefore, the improvement in fatigue properties of magnesium alloys is of great interest.

During the smelting process of metals, casting defects (i.e. porosity, oxide films and inclusions) are usually formed and deteriorate the fatigue properties of the castings [14–16]. With the development of casting technologies and Mg–RE alloys [17–19], more and more defect-free Mg castings have been produced. Fatigue properties of defect-free magnesium alloys are mainly dependent on their microstructures [20–22]. Generally, RE elements exist in Mg–RE alloys in three forms: second phase particles, solid solution and precipitates [23–25]. Different heat treatment processes lead to different microstructures, which significantly influences their fatigue properties and fracture behaviour. Taking Mg–3Nd–0.2Zn–0.5Zr (NZ30K) alloy

Z.-M. Li, H. Zou,
Institute of Sci-technology Strategy, Jiangxi Academy of Sciences, Nanchang 330096, China

Z.-M. Li
Zhejiang Jinfei Kaida Wheel Co., Ltd, Jinhua 321000, China

J.-C. Dai
Research Institute (R & D Center), Shanghai JuneBang Technology Corporation, Shanghai 200032, China

B.-L. Liu*
National Engineering Research Center of Light Alloy Net Forming, Shanghai 200240, China
e-mail: bojin516@aliyun.com

J.-P. Pan
National Engineering Research Center of Light Alloy Net Forming, Shanghai Jiao Tong University, Shanghai 200240, China

as an example, in the as-cast state, Nd mainly exists in the secondary phase particles distributed at grain boundaries. After solution treatment, the secondary phase particles disappear and Nd is dissolved into the matrix and exists in the form of solid solution atoms [23]. Further ageing treatment after solution causes the dissolved Nd atoms to precipitate, which leads to higher fatigue strength (~ 85 MPa) than that of the as-cast and T4-treated conditions (~ 70 MPa) [17, 26]. Furthermore, different ageing treatment conditions cause the formation of different precipitates such as β″ (T6: 540 °C × 10 h + 200 °C × 14 h) and β′ (T7: 540 °C × 10 h + 250 °C × 10 h) [23], which leads to different fatigue strengths [26].

Though the effect of heat treatment on high-cycle fatigue of cast Mg alloy containing Nd has been extensively reported [17, 26], comprehensive investigation of the influence of ageing treatment on the low-cycle fatigue (LCF) behaviour of the Mg–Nd alloy is yet to be reported. This study aims to investigate LCF characteristics of the $Mg_{96.47}Nd_{2.9}Zn_{0.21}$ alloy containing 0.42Zr under peak-aged ($T6_1$: 540 °C × 8 h + 200 °C × 14 h) and over-aged ($T6_2$: 540 °C × 8 h + 200 °C × 400 h) conditions and then to predict the fatigue life of the alloys using the energy density [27].

2 Experimental

A direct chill casting (casting speed of 100 mm·min^{-1}, water flow of 25 L·min^{-1} and casting temperature of 730 °C) $Mg_{96.3}Nd_3Zn_{0.2}Zr_{0.5}$ ingot (70 mm in diameter and 2000 mm in length) was used. In this work, the alloy was supplied by National Engineering Research Center of Light Alloys Net Forming and Shanghai Jiao Tong University. The actual chemical composition of the alloy was measured to be $Mg_{96.47}Nd_{2.9}Zn_{0.21}Zr_{0.42}$ by an Optima 7300DV inductively coupled plasma analysis (ICP). Blanks with dimensions of 16 mm × 16 × mm × 140 mm were cut along the length direction of the ingot for tensile and fatigue test samples. Both peak-aged ($T6_1$: 540 °C × 8 h + 200 °C × 14 h) and over-aged ($T6_2$: 540 °C × 8 h + 200 °C × 400 h) samples were prepared (Fig. 1).

Room temperature (RT) tensile specimens with gage dimensions Φ6 mm × 30 mm were prepared and then tested using an Instron 5566 tensile machine. For the tensile testing, the crosshead speed of about 1 mm·min^{-1} was adopted. The LCF test specimens with gage dimensions Φ6mm × 12 mm were prepared and electrolytically polished to improve the surface quality; then, the fatigue testing was carried out using an Instron 8802 fatigue machine under the strain-controlled mode (triangular waveform of $R = -1$, frequency of 1 Hz, total strain amplitude in the range of 0.2%–0.6%). Under each condition, three specimens were tested and the average value was employed as the final result. At strain amplitude levels of 0.2% and 0.3%, the fatigue testing was lasted for 104 cycles under the strain-controlled mode, and then, it was converted to the stress-controlled mode (sinusoidal loading of $R = -1$, frequency of 30 Hz) for 107 cycles or until the failure of the specimen. Furthermore, some fatigue testing was performed under the constant stress amplitude of 90 MPa (high-cycle fatigue, HCF) until failure for comparison.

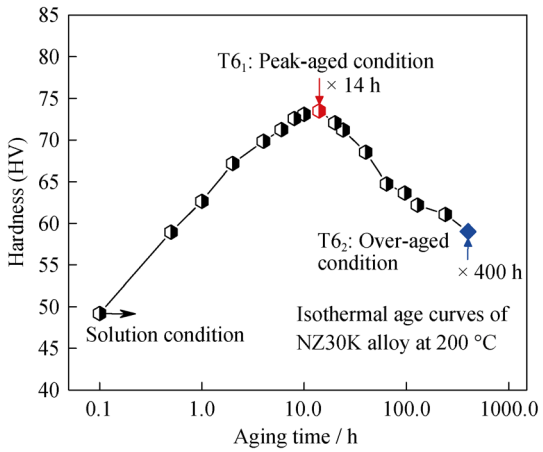

Fig. 1 Variation in hardness of NZ30K alloy samples as a function of time during isothermal aging at 200 °C

The samples for the microstructural observation were chemically etched in an acetic–picric solution (20 ml acetic acid, 60 ml ethanol, 1 ml nitric acid and 19 ml water) and then characterized using an Olympus optical microscope (OM). The fracture surfaces of the fatigue samples were examined using a FEI 250 scanning electron microscope (SEM). The initiation and propagation behaviours of the fatigue cracks on the sample surface were investigated using SEM and OM, respectively.

3 Results and discussion

3.1 Theoretic analysis

Figure 2 shows microstructures of $T6_1$- and $T6_2$-treated $Mg_{96.47}Nd_{2.9}Zn_{0.21}$ alloys containing 0.42Zr. The average grain size of the alloys is measured to be 52 ~ 56 μm. The beta precipitates are very small, smaller than 200 nm in size, and they cannot be observed in Fig. 2. They can be characterized using transmission electron microscopy (TEM) as Fu [28] reported. In the optical micrographs, other than Mg matrix, only Zr-rich zones (dark areas within grains and at grain boundaries) and some small Zr-containing particles distribute at grain boundaries [29, 30].

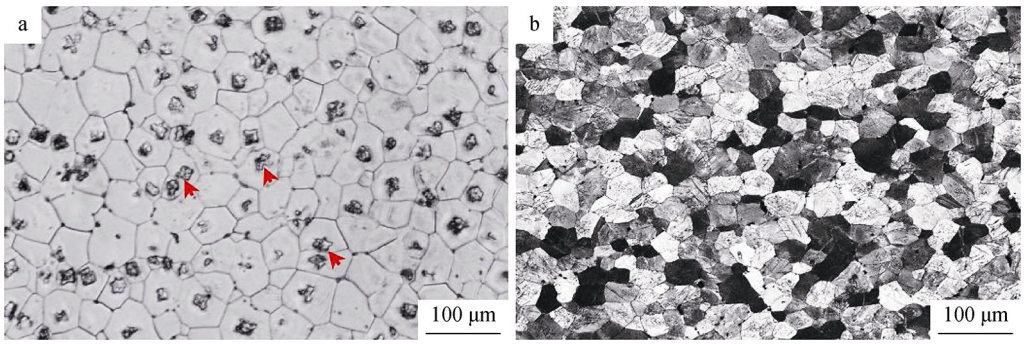

Fig. 2 OM images of $Mg_{96.47}Nd_{2.9}Zn_{0.21}Zr_{0.42}$ alloys under **a** $T6_1$-treated and **b** $T6_2$-treated conditions

Compared with the $T6_1$-treated counterpart, $T6_2$-treated alloy shows interesting microstructure. The grains with different orientations have different contrasts after etching. Fu [28] pointed that the precipitates in $T6_2$-treated alloy are similar to those in the T7-treated counterpart (540 °C × 8 h + 250 °C × 10 h). In the $T6_1$-treated condition, the fine plate-shaped β″ precipitates with DO_{19} structure (a = 0.64 nm, c = 0.52 nm) are the dominant strengthening phase, while β′ precipitates with fcc structure (a = 0.742 nm) are the dominant phase in $T6_2$-treated alloy [23]. The β″ precipitates have smaller size and higher density than the β′ precipitates.

Table 1 shows RT tensile properties of $T6_1$- and $T6_2$-treated $Mg_{96.47}Nd_{2.9}Zn_{0.21}Zr_{0.42}$ alloys, and their logarithmic strain–true stress curves are shown in Fig. 3. The alloys exhibit similar yield strength (YS of ∼ 150 MPa) and ultimate tensile strength (UTS of ∼ 300 MPa), while $T6_2$-treated alloy has a better ductility (elongation of ∼ 12.6%) than $T6_1$-treated counterpart (elongation of ∼ 7.1%).

3.2 Cyclic stress response and strain resistance

It was reported that the variations in the stress value and plastic strain value during LCF testing are important [21]. Figure 4a shows the relationship between stress amplitude (σ_{T6_1} and σ_{T6_2}) and number of cycles (N_f) for $T6_1$- and $T6_2$-treated $Mg_{96.47}Nd_{2.9}Zn_{0.21}Zr_{0.42}$ alloys at different strain values (0.2%, 0.3% and 0.5%). Table 2 shows the initial and maximum stress amplitudes ($\Delta\sigma_I$ and $\Delta\sigma_M$, respectively) of the samples at different strain values. Apparently, the stress amplitude increases with the increase in the total strain value, and the stress value at the strain value of 0.6% is ∼ 88 MPa ($T6_1$) and ∼ 81 MPa ($T6_2$), higher than that at the strain value of 0.2%. At the strain value of 0.2%, the stress amplitudes of both the $T6_1$- and $T6_2$-treated alloys keep steady during fatigue testing. When the strain value increases to 0.3%, the stress of $T6_1$-treated alloy increases and subsequently decreases with the increase in cyclic number, while that of $T6_2$-treated counterpart increases slightly during the cyclic loading. On the contrary, at the same strain value, the two aged alloys exhibit the similar initial stress amplitudes. For instance, at the strain value of 0.4%, the maximum stress amplitudes of $T6_1$- and $T6_2$-treated alloys are 146 and 125 MPa, respectively, increased by 22 and 2 MPa than those at the first cycle (123–124 MPa), indicating that $T6_1$-treated alloy could be hardened more than $T6_2$-treated counterpart during fatigue. Figure 4b plots the mean stress against the number of cycles for $T6_1$- and $T6_2$-treated samples. For both samples, the mean stress remains steady. The mean stress of the alloys tested at different stain values is about − 1.01–2.47 MPa ($T6_1$) and − 1.41–3.85 MPa ($T6_2$), respectively. Therefore, the influence of ageing treatment and strain value on mean stress of the alloys is very marginal.

Figure 4c illustrates the variation in plastic strain amplitude for the alloys during fatigue testing. The increase in the total strain amplitude leads to the increase in the plastic strain value. At the strain amplitude of 0.2%, the plastic strain values of both $T6_1$- and $T6_2$-treated alloys remain steady during the entire fatigue testing. When the total strain amplitude is above 0.3%, the plastic strain amplitude of $T6_2$-treated samples slightly decreases before failure. For $T6_1$-treated sample, as the total strain amplitude increases to 0.4%, the plastic strain amplitude decreases and subsequently increases. At the same strain value, the $T6_2$-treated sample has a higher plastic strain amplitude than $T6_1$-treated counterpart, corresponding to a lower stress response in $T6_2$ condition.

Table 1 Tensile properties of $T6_1$- and $T6_2$-treated $Mg_{96.47}Nd_{2.9}Zn_{0.21}Zr_{0.42}$ alloys

States	YS/MPa	UTS/MPa	Elongation/%
$T6_1$	152	302	7.1
$T6_2$	151	300	12.6

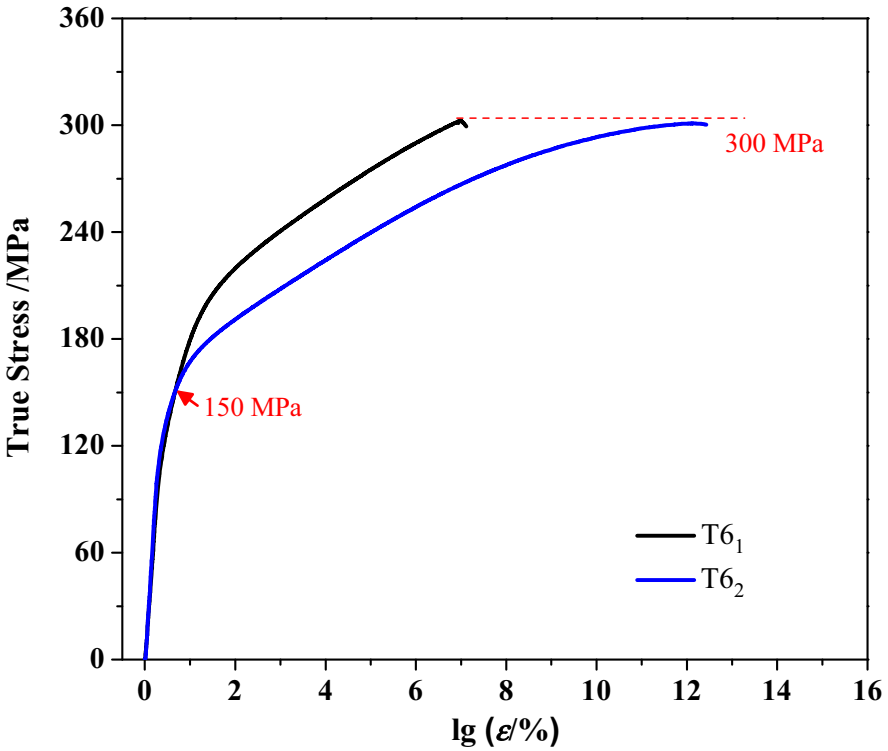

Fig. 3 Logarithmic strain–true stress curves of the $T6_1$- and $T6_2$-treated $Mg_{96.47}Nd_{2.9}Zn_{0.21}Zr_{0.42}$ alloys

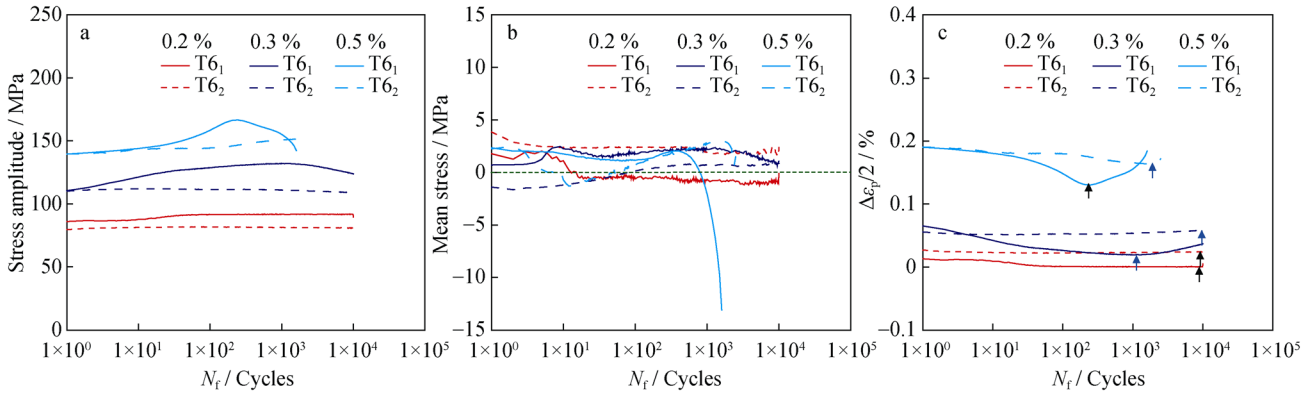

Fig. 4 Variation in **a** stress amplitude and **b** mean stress with number of cycles (N_f) for $T6_1$- and $T6_2$-treated $Mg_{96.47}Nd_{2.9}Zn_{0.21}Zr_{0.42}$ alloys; **c** variations in plastic stain amplitude ($\Delta\varepsilon_p/2$) during cyclic deformation for alloys

3.3 Hysteresis loop and energy density

It is widely acknowledged that the hysteresis loop (or hysteresis energy) is an important fatigue parameter for magnesium alloys [27, 31]. Figure 5a shows stress–strain hysteresis loops of $T6_1$- and $T6_2$-treated alloys at different cyclic numbers (at the total strain amplitude of 0.4%). For comparison, the compressive tips of the hysteresis loops of the alloys tested at the total strain value of 0.4% were translated to the origin of the coordinates in Fig. 5a. It can be seen that the shape of hysteresis loops of both $T6_1$- and $T6_2$-treated samples is nearly symmetrical during the entire fatigue testing. Figure 5b shows relationship between total strain energy density (ΔW_t) or plastic strain energy density (ΔW_p) and cyclic number (N_f) of the alloys at strain value of 0.4%. The value of ΔW_p of $T6_1$-treated sample keeps steady, decreases and then increases, while that of $T6_2$-treated counterparts always remains steady during the fatigue testing. When the cyclic number is below 100, ΔW_p value of $T6_2$-treated alloy is equivalent to that of $T6_1$-treated counterpart. By further increasing the number of cycles, ΔW_p value of $T6_1$ alloy is lower than that of $T6_2$ alloy. In contrast, ΔW_t values of the two age-treated alloys are close. Similar results are also observed in the

specimens tested at different total strain amplitudes, as shown in Fig. 5c. In addition, the increase in the total strain amplitude leads to the increase in both ΔW_t and ΔW_p values. The LCF lives of the two treated alloys are also close, which might be because that the values of ΔW_t for them are close.

3.4 Fatigue life

It is well known that the LCF lives of the magnesium alloys could be described based upon the Coffin–Manson relation and Basquin laws as follows [3]:

$$\frac{\Delta\varepsilon_t}{2}=\frac{\Delta\varepsilon_e}{2}+\frac{\Delta\varepsilon_p}{2}=\frac{\Delta\sigma}{2E}+\left(\frac{\Delta\sigma}{2K'}\right)^{1/n'}=\frac{\sigma_f'(2N_f)^b}{E}+\varepsilon_f'(2N_f)^c \quad (1)$$

where $\Delta\varepsilon_t$, $\Delta\varepsilon_e$ and $\Delta\varepsilon_p$ are true strain range, true elastic strain range and true plastic strain range, respectively; E and $\Delta\sigma$ are elastic modulus and true stress range, respectively; n', b, c, K', σ_f and ε_f are cyclic strain hardening exponent, fatigue strength exponent, fatigue ductility exponent, cyclic strength coefficient, fatigue strength coefficient and fatigue ductility coefficient, respectively. Figure 6a shows strain life curves of $T6_1$- and $T6_2$-treated alloys. At the same strain amplitude, the fatigue lives of the two alloys are close. The parameters in Eq. (1) were calculated by fitting the relationship between $\lg(\Delta\sigma/2)$ and $\lg(\Delta\varepsilon_p/2)$, $\lg(\Delta\sigma/2)$ and $\lg(2N_f)$, $\Delta\varepsilon_p/2$ and $\lg(2N_f)$, and the results are shown in Table 3. The LCF lives were predicted based on Eq. (1) and fit well with the experimental data as shown in Fig. 6a; thus, Eq. (1) and the parameters obtained from $T6_1$-treated samples could be used to describe the strain–life curves of both $T6_1$- and $T6_2$-treated alloys.

Table 2 Cyclic stress amplitudes of $T6_1$- and $T6_2$-treated $Mg_{96.47}Nd_{2.9}Zn_{0.21}Zr_{0.42}$ alloys at strains of 0.2%–0.6% (MPa)

Parameters	States	0.2%	0.3%	0.4%	0.5%	0.6%
σ_I	$T6_1$	86	110	124	139	156
	$T6_2$	81	110	123	139	155
$\Delta\sigma_I=\sigma_{T6_1}-\sigma_{T6_2}$		5	0	1	0	1
σ_M	$T6_1$	92	132	146	166	180
	$T6_2$	82	112	125	151	163
$\Delta\sigma_M=\sigma_{T6_1}-\sigma_{T6_2}$		10	20	21	15	17
$\Delta\sigma=\sigma_M-\sigma_I$	$T6_1$	6	22	22	27	24
	$T6_2$	2	2	2	12	8

It has been reported that both plastic strain and total strain energy densities could be used to predict the LCF lives of magnesium alloys as follows [31]:

$$N_f=(C/\Delta W_p)^{1/m} \quad (2)$$

$$N_f=(C/\Delta W_t)^{1/m} \quad (3)$$

where m and C are constants. Figure 6b shows the predicted life curves based on Eqs. (2), (3) and experimental data. The values of m and C are determined to be $\sim$ 0.64 and 48 $MJ\cdot m^{-3}$ in Eq. (2) and 0.35 and 10 $MJ\cdot m^{-3}$ in Eq. (3), respectively. It can be seen that the predicted values fit well with the experimental results, indicating that the parameters obtained from $T6_1$-treated alloy could be also used to predict the fatigue life of $T6_2$-treated counterpart.

Weibull data in Fig. 7a show the influence of ageing treatment on HCF life of NZ30K alloys. The fatigue data in Fig. 7a point plot linearly well $\ln\ln\{1/[1-F_w(N_f)]\}$ vs. $\ln(N_f)$, where F_w is 63% probability of failure and N_f is the fatigue life data) [16]. The characteristic fatigue life (N_0) of $T6_1$-treated alloy is $\sim 3.22\times10^6$ cycles at the stress amplitude of 90 MPa, approximately twice that of $T6_2$-treated counterpart.

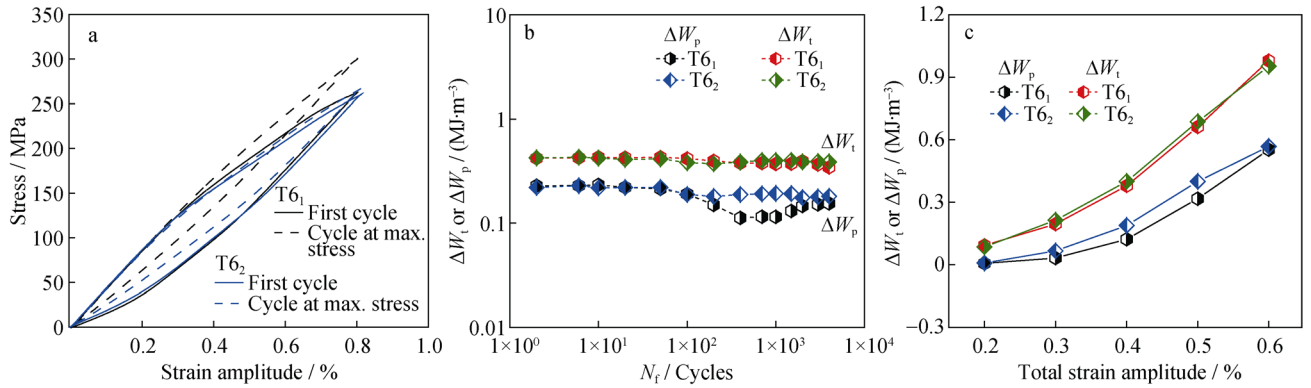

Fig. 5 **a** Stress–strain hysteresis loops at total strain amplitude of 0.4%; **b** variation in total strain energy density (ΔW_t) and plastic strain energy density (ΔW_p) with number of cycles for $T6_1$- and $T6_2$-treated NZ30K alloys tested at total strain amplitude of 0.4%; **c** relationship between ΔW_p or ΔW_t and total strain amplitude for $Mg_{96.47}Nd_{2.9}Zn_{0.21}Zr_{0.42}$ alloys

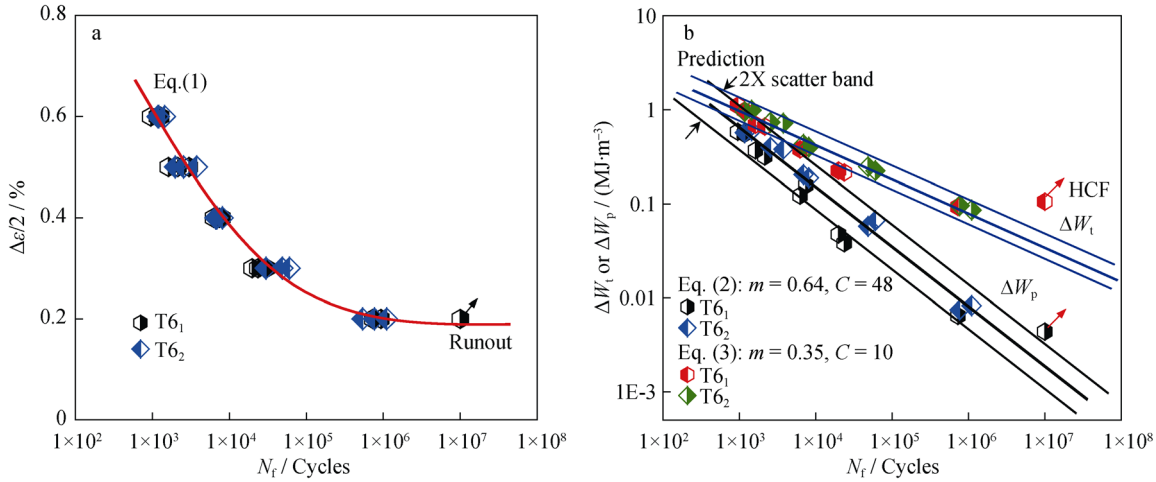

Fig. 6 **a** Strain life curves of $T6_1$- and $T6_2$-treated $Mg_{96.47}Nd_{2.9}Zn_{0.21}Zr_{0.42}$ alloys and **b** predicted low-cycle fatigue lives using Eqs. (2) and (3)

Table 3 Low-cycle fatigue parameters of $T6_1$- and $T6_2$-treated $Mg_{96.47}Nd_{2.9}Zn_{0.21}Zr_{0.42}$ alloys

States	n'	K'/MPa	b	ε_f'/%	c	σ_f'/MPa
$T6_1$	0.12	363	− 0.1	68.4	− 0.78	376
$T6_2$	0.22	598	− 0.1	8.5	− 0.45	354

Figure 7b shows true stress–true strain hysteresis loops of $T6_1$- and $T6_2$-treated $Mg_{96.47}Nd_{2.9}Zn_{0.21}Zr_{0.42}$ alloys at the maximum stress values of 90 ~ 92 MPa. $T6_1$-treated alloy has lower hysteresis energies than $T6_2$-treated counterpart. The higher hysteresis energy was reported to correspond to higher fatigue damage and shorter fatigue life [27]. Therefore, longer fatigue life of $T6_1$-treated $Mg_{96.47}Nd_{2.9}Zn_{0.21}Zr_{0.42}$ alloy tested at stress-controlled loading appears to be due to its lower hysteresis energy and higher matrix strength.

3.5 Fatigue failure and cyclic deformation behaviour

Figure 8 shows SEM images of fatigue crack initiation regions of $T6_1$- and $T6_2$-treated $Mg_{96.47}Nd_{2.9}Zn_{0.21}Zr_{0.42}$ alloys. For both alloys, the fatigue failure is mainly originated from the isolated facets within one or two grains located on the surface of the specimens rather than casting flaws. Figure 9 shows fatigue crack initiation and growth path of a small crack on the surface of the alloys. In the peak-aged alloys, precipitates contribute to the cyclic response other than the grain boundary. Both basal and non-basal slip bands are observed on the surface of the peak-aged sample under the continuous loading. It was reported that addition of Nd and Zn would promote the activation of non-basal slip systems [32]. The fatigue crack initiates from the cracked persistent slip bands (PSBs), which is due to the intrusion/extrusion of dislocations–slip and cumulative damage. The cyclic hardening and subsequent softening behaviour in the peak-aged sample might be primarily due to the retarding effect of the fine β'' precipitates on the dislocations–slip and the formation of cracks on the surface of the sample, respectively. In contrast, for the over-aged sample, the fatigue cracks initiate from the cracked grain boundaries. With the increase in the dislocations piled up at grain boundaries, the grain boundaries start to glide to coordinate the deformation and release stress. Continued grain boundary sliding would accelerate the crack of the grain boundary under continuous loading. The interaction mode between precipitates with gliding dislocations is associated with size and number density of the precipitates. The cyclic stress amplitude of the over-aged alloy keeps steady during fatigue testing, which might be due to the relatively homogenous deformation. The cracks in $T6_1$-treated sample tend to propagate along the cracked PSBs within grains in the trans-granular mode, while those in $T6_2$-treated counterpart propagate along the cracked grain boundaries in the inter-granular mode.

4 Conclusion

The peak-aged and over-aged $Mg_{96.47}Nd_{2.9}Zn_{0.21}$ alloys containing 0.42Zr have close yield strength and ultimate tensile strength, and $T6_2$-treated alloy has higher ductility and plastic strain amplitude, but lower cyclic stress response than $T6_1$-treated counterpart.

The influence of ageing treatment on LCF lives of the NZ30K alloys is very marginal, which is attributed to similar total strain energy densities in $T6_1$- and $T6_2$-treated alloys. In contrast, the ageing treatment significantly

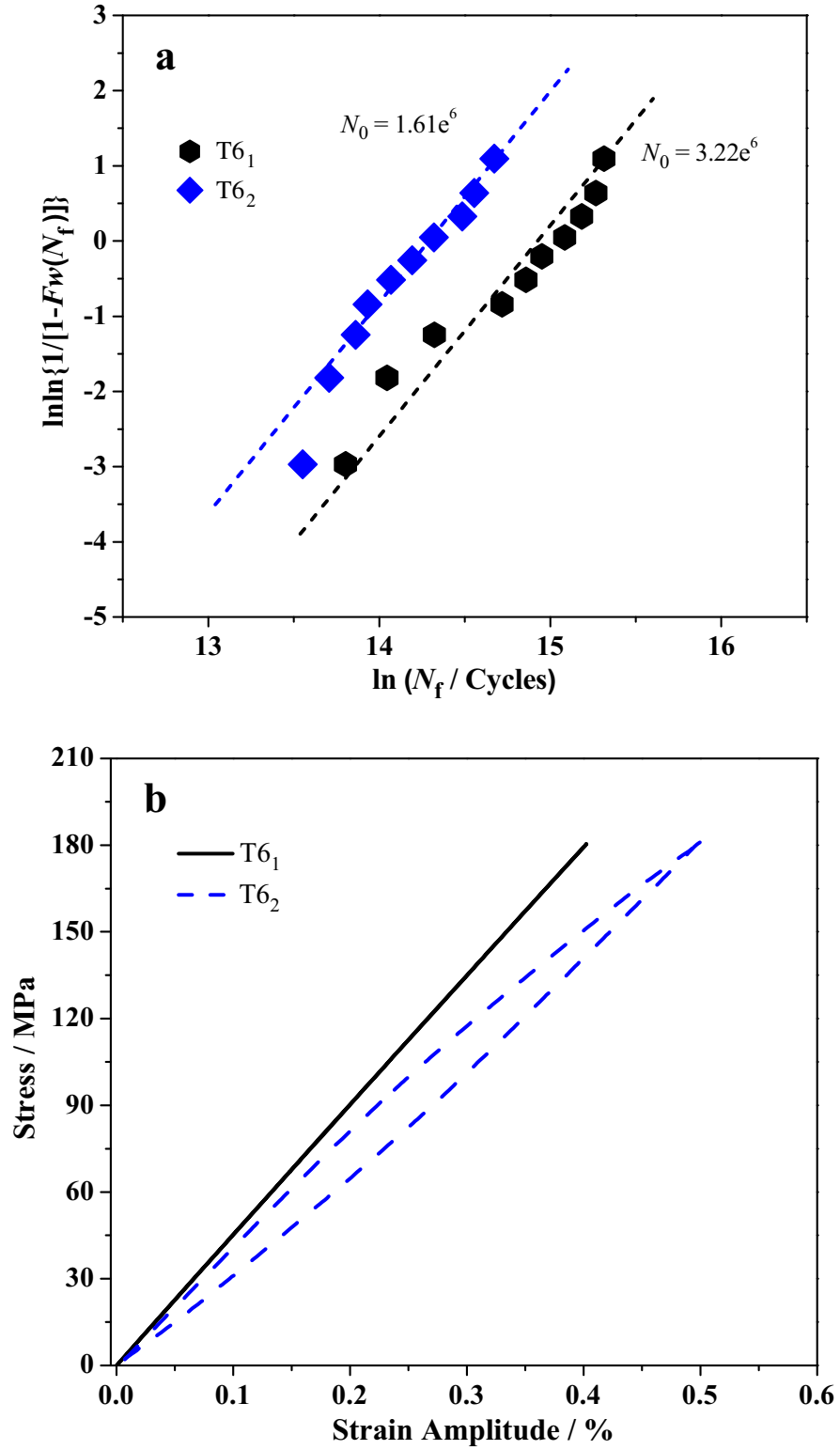

Fig. 7 **a** Weibull plots showing influence of ageing treatment on HCF life of the $Mg_{96.47}Nd_{2.9}Zn_{0.21}Zr_{0.42}$ alloys and **b** true stress–true strain hysteresis loops at maximum stress values of 90–92 MPa and strain values of ~ 0.20% ($T6_1$) and ~ 0.25% ($T6_2$)

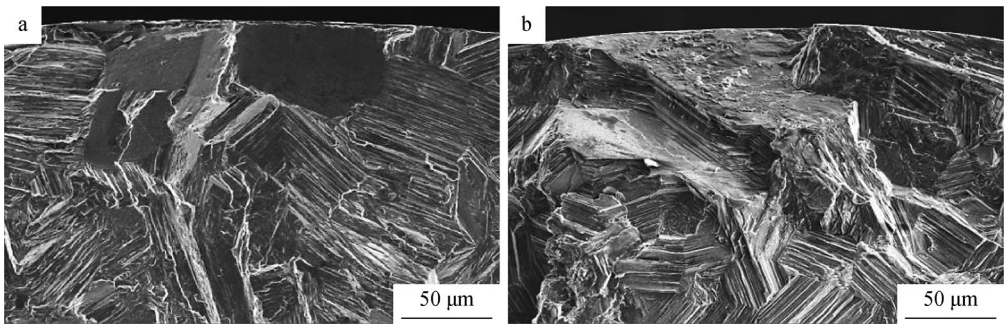

Fig. 8 SEM images of fatigue crack initiation region in **a** $T6_1$- and **b** $T6_2$-treated $Mg_{96.47}Nd_{2.9}Zn_{0.21}Zr_{0.42}$ alloys

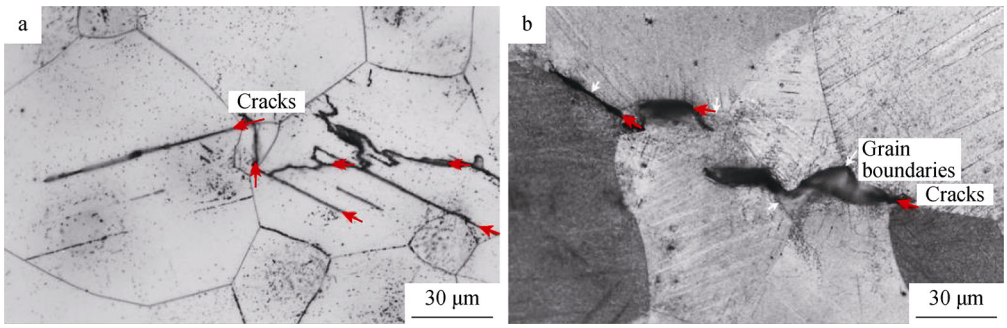

Fig. 9 OM images of fatigue crack initiation and growth path of a small crack in **a** $T6_1$- and **b** $T6_2$-treated $Mg_{96.47}Nd_{2.9}Zn_{0.21}Zr_{0.42}$ alloys

affects the HCF lives of the alloys. The shorter fatigue life of $T6_2$-treated alloy compared with that of $T6_1$-treated counterpart is attributed to the higher hysteresis energy in the over-aged condition. In addition, the LCF lives of the aged $Mg_{96.47}Nd_{2.9}Zn_{0.21}Zr_{0.42}$ alloys can be predicted using the Coffin–Manson relation and Basquin laws, the energy-based concepts, respectively.

For $T6_2$-treated alloy, the stress amplitude slightly increases, which is due to its high ductility and homogenous deformation. In $T6_1$ state, the fatigue cracks initiate along the cracked PSBs and then propagate in the transgranular mode, while in $T6_2$ state, the fatigue cracks initiate along grain boundaries and then propagate in the intergranular mode.

Acknowledgements This work was financially supported by the Key Research Project of Jiangxi Academy of Sciences (No.2017–YZD2–03), the Introduction Doctoral Program of Jiangxi Academy of Sciences (No. 2016–YYB–09) and the Collaborative innovation GSP Project of Jiangxi Academy of Sciences (No. 2016–XTPH1–09). The authors are grateful to Prof. Qigui Wang (General Motors Company) and Prof. Alan A. Luo (Ohio State University) for their helpful discussions. The authors are also grateful to Prof. Liming Peng and Dr. Penghuai Fu (SJTU) for providing the Mg–Nd alloy. The authors also acknowledge Shanghai Jiao Tong University for access to experimental facilities and thank Dr. Haiyan Yue at Shanghai Jiao Tong University for her SEM analysis.

References

[1] Yang Y, Zhang K, Ma ML, Yuan JW. Microstructure and phase compositions of as-cast Mg–3.9Zn–0.6RE (Gd, Y) alloy with different Gd/Y ratios. Rare Met. 2015;34(3):160.
[2] Li D, Xue HS, Yang G, Zhang DF. Microstructure and mechanical properties of Mg–6Zn–0.5Y magnesium alloy prepared with ultrasonic treatment. Rare Met. 2017;36(8):622.
[3] Zhang ZQ, Liu X, Hu WY, Li JH, Le QC, Bao L, Zhu ZJ, Cui JZ. Microstructures, mechanical properties and corrosion behaviors of Mg–Y–Zn–Zr alloys with specific Y/Zn mole ratios. J Alloys Compd. 2015;624:116.
[4] Chen Q, Shu DY, Zhao ZD, Zhao ZX, Wang YB, Yuan BG. Microstructure development and tensile mechanical properties of Mg–Zn–RE–Zr magnesium alloy. Mater Des. 2012;40(40):488.
[5] Singh LK, Joseph P, Srinivasan A, Pillai UTS, Pai BC. Microstrucure and mechanical properties of gadolinium- and misch metal added Mg–Al alloy. Rare Met. 2017. https://doi.org/10.1007/s12598-017-0928-3.
[6] Mokdad F, Chen DL. Strain-controlled low cycle fatigue properties of a rare-earth containing ZEK100 magnesium alloy. Mater Des. 2015;67:436.
[7] Zhang P, Li ZM, Yue HY. Strain-controlled cyclic deformation behavior of cast Mg–2.99Nd–0.18Zn–0.38Zr and AZ91D magnesium alloys. J Mater Sci. 2016;51(11):5469.
[8] Jiang HS, Zheng MY, Qiao XG, Wu K, Peng QY, Yang SH, Yuan YH, Luo JH. Microstructure and mechanical properties of WE43 magnesium alloy fabricated by direct-chill casting. Mater Sci Eng A. 2017;684:158.
[9] Lan AY, Huo LF. Effect of substitution of minor Nd for Y on mechanical and damping properties of heat-treated Mg–Zn–Y–Zr alloy. Mater Sci Eng A. 2016;651:646.

[10] Feng H, Liu HP, Cao H, Yang Y, Xu YC, Guan JY. Effect of precipitates on mechanical and damping properties of Mg–Zn–Y–Nd alloys. Mater Sci Eng A. 2015;639:1.
[11] Li HZ, Lv F, Xiao ZY, Liang XP, Sang FJ, Li PW. Low-cycle fatigue behavior of a cast Mg–Y–Nd–Zr alloy by T6 heat treatment. Mater Sci Eng A. 2016;676:377.
[12] Hazeli K, Askari H, Cuadra J, Streller F, Carpick RW, Zbib HM, Kontsos A. Microstructure-sensitive investigation of magnesium alloy fatigue. Int J Fatigue. 2015;68:55.
[13] He ZL, Peng LM, Fu PH, Wang YX, Hu XY, Ding WJ. High cycle fatigue improvement by heat-treatment for semi-continuous casting $Mg_{96.34}Gd_{2.5}Zn_1Zr_{0.16}$ alloy. Mater Sci Eng A. 2014; 604(15):78.
[14] Wang SD, Xu DK, Wang BJ, Han EH, Dong C. Effect of corrosion attack on the fatigue behavior of an as-cast Mg–7% Gd–5%Y–1%Nd–0.5%Zr alloy. Mater Des. 2015;84(3–4):185.
[15] Li X, Xiong SM, Guo Z. Failure behavior of high pressure die casting AZ91D magnesium alloy. Mater Sci Eng A. 2016;672: 216.
[16] Li ZM, Fu PH, Peng LM, Wang YX, Jiang HY, Wu GH. Comparison of high cycle fatigue behaviors of Mg–3Nd–0.2 Zn–Zr alloy prepared by different casting processes. Mater Sci Eng A. 2013;579(9):170.
[17] Peng LM, Fu PH, Li ZM, Yue HY, Li DY, Wang YX. High cycle fatigue behaviors of low pressure cast Mg–3Nd–0.2 Zn–2Zr alloys. Mater Sci Eng A. 2014;611(9):170.
[18] Fang XG, Lü SL, Zhao L, Wang J, Liu LF, Wu SS. Microstructure and mechanical properties of a novel Mg–RE–Zn–Y alloy fabricated by rheo-squeeze casting. Mater Des. 2016;94:353.
[19] He ZL, Fu PH, Wu YJ, Peng LM, Zhang Y, Li ZM. High cycle fatigue behavior of as-cast $Mg_{96.34}Gd_{2.5}Zn_1Zr_{0.16}$ alloy fabricated by semi-continuous casting. Mater Sci Eng A. 2013; 587(1):72.
[20] Dong J, Liu WC, Song X, Zhang P, Ding WJ, Korsunsky AM. Influence of heat treatment on fatigue behaviour of high-strength Mg–10Gd–3Y alloy. Mater Sci Eng A. 2010;527(21):6053.
[21] Mirza FA, Chen DL, Li DJ, Zeng XQ. Cyclic deformation behavior of a rare-earth containing extruded magnesium alloy: effect of heat treatment. Metall Mater Trans A. 2015;46(3):1168.
[22] Mokhtarishirazabad M, Azadi M, Farrahi GH, Winter G, Eichlseder W. Improvement of high temperature fatigue lifetime in AZ91 magnesium alloy by heat treatment. Mater Sci Eng A. 2013;588(5):357.
[23] Fu PH, Peng LM, Jiang HY, Chang JW, Zhai CQ. Effects of heat treatments on the microstructures and mechanical properties of Mg–3Nd–0.2Zn–0.4Zr (wt.%) alloy. Mater Sci Eng A. 2008; 486(1):183.
[24] Su CY, Li DJ, Ying T, Zhou LP, Li L, Zeng XQ. Effect of Nd content and heat treatment on the thermal conductivity of Mg–Nd alloys. J Alloys Compd. 2016;685:114.
[25] He SM, Zeng XQ, Peng LM, Gao X, Nie JF, Ding WJ. Microstructure and strengthening mechanism of high strength Mg–10Gd–2Y–0.5Zr alloy. J Alloys Compd. 2007;427(1):316.
[26] Li ZM, Wang QG, Luo AA, Peng LM, Zhang P. Fatigue behavior and life prediction of cast magnesium alloys. Mater Sci Eng A. 2015;647:113.
[27] Lv F, Yang F, Li SX, Zhang ZF. Effects of hysteresis energy and mean stress on low-cycle fatigue behaviors of an extruded magnesium alloy. Scr Mater. 2011;65(1):53.
[28] Fu PH. Study on the Microstructure, Mechanical Properties and Strengthen Mechanism of Mg–Nd–Zn–Zr Alloys. Shanghai: Shanghai Jiao Tong University; 2009. 102.
[29] Fu PH, Peng LM, Jiang HY, Zhai CQ, Gao X, Nie JF. Zr-containing precipitates in Mg–3wt%Nd–0.2wt%Zn–0.4wt%Zr alloy during solution treatment at 540 °C. Mater Sci Forum. 2007; 546:97.
[30] Bettles CJ, Gibson MA, Zhu SM. Microstructure and mechanical behaviour of an elevated temperature Mg-rare earth based alloy. Mater Sci Eng A. 2009;505(1):6.
[31] Park SH, Hong SG, Lee BH, Bang W, Lee CS. Low-cycle fatigue characteristics of a rolled Mg–3Al–1Zn alloy. Int J Fatigue. 2010;32(1):1835.
[32] Fu PH, Peng LM, Nie JF, Jiang HY, Ma L, Bourgeois L. Ductility improvement of Mg–Nd–Zr cast alloy by trace addition of Zn. Mater Sci Forum. 2011;690:230.